Mechanics Research Communications xxx (2012) xxx–xxx

Contents lists available at SciVerse ScienceDirect

Mechanics Research Communications

journal homepage: www.elsevier.com/locate/mechrescom

Medical image-based simulation of abdominal aortic aneurysm growth

S. Zeinali-Davarani, S. Baek*

Department of Mechanical Engineering, Michigan State University, East Lansing, MI 48824-1224, United States

ARTICLE INFO

Article history:
Received 18 August 2011
Received in revised form 3 January 2012
Available online xxx

Keywords:
Vascular growth and remodeling
Patient-specific modeling
Aneurysm rupture
Finite element analysis
Inverse optimization

ABSTRACT

Advances in theoretical modeling of biological tissue growth and remodeling (G&R) and computational biomechanics have been helpful to capture salient features of vascular remodeling during the progression of vascular diseases. Nevertheless, application of such advances to individualized diagnosis and clinical treatment of diseases such as abdominal aortic aneurysm (AAA) remains challenging. As a step toward that goal, in this paper, we present a computational framework necessary towards patient-specific modeling of AAA growth. Prior to AAA simulations, using an inverse optimization method, initial material parameters are identified for a healthy aorta such that a homeostatic condition is satisfied for the given medical image-based geometrical model under physiological conditions. Various shapes of AAAs are then computationally created by inducing elastin degradation with different spatio-temporal distributions. The simulation results emphasize the role of extent of elastin damage, geometric complexity of an enlarged AAA, and sensitivity of stress-mediated collagen turnover on the wall stress distribution and the rate of expansion. The results also show that the distributions of stress and local expansion initially correspond to the extent of elastin damage, but change via stress-mediated tissue G&R depending on the aneurysm shape. Finally, we suggest that the current framework can be utilized along with medical images from an individual patient to predict the AAA shape and mechanical properties in the near future via an inverse scheme.

1. Introduction

Abdominal aortic aneurysm (AAA) affects about 5% of elderly men in the US. Its rupture and the risk associated with its treatment pose an enormous social and economic burden in our aging society and there has been continuous demand for better risk assessment and patient management based on advances in medical imaging and computational biomechanics.

Classical finite element (FE) analysis using a nonlinear constitutive model of vascular wall and a medical image-based geometric model provides a better estimation of wall stress as a more reliable biomarker of rupture (Dorfmann et al., 2010; Fillinger et al., 2002; Raghavan and Vorp, 2000; Rissland et al., 2009; Speelman et al., 2007). These previous studies, however, estimate stress distribution of an AAA at a fixed time and do not account for the continuous evolution in material properties, and thus, strength of the wall.

Arterial wall exhibits remarkable ability to adapt in response to changes in mechanical environment (Driss et al., 1997; Jackson et al., 2005; Mulvany, 1992). The need to understand the role of mechanical stimuli in vascular adaptation has motivated many theoretical models of vascular growth and remodeling (G&R), incorporated within FE method framework (Baek et al., 2006; Figueroa et al., 2009; Watton et al., 2004; Watton and Hill, 2009; Kroon and Holzapfel, 2007, 2009; Hariton et al., 2007). These G&R simulations use microstructural information of structural constituents (i.e. collagen, elastin and smooth muscle (SM)) at a given time to calculate the mechanical state (e.g. stress or strain) and update the microstructural properties of constituents by continuous mechano-sensitive turnover of constituents.

There have been two different G&R models developed for simulating the progression of AAAs: first by Watton et al. (2004), Watton and Hill (2009) and recently by Zeinali-Davarani et al. (2011b,c). Although the detail formulations are different, they both employ a similar constrained mixture approach; a removal of elastin initiates an AAA and the AAA expands with stress(or strain)-mediated turnover of collagen fibers. Both studies capture salient features of G&R of AAAs, i.e. fragmented and diminished elastin commonly reported in AAAs, and the mechanism by which a stiff, collagenous tissue expands. The later study, however, focuses on further improvement of the G&R computational framework to incorporate geometrical models constructed from medical images. Briefly, Zeinali-Davarani et al. (2011c) first extended an existing FE model of stress-medicated G&R of arteries (Baek et al., 2006) to incorporate a medical image-based geometry of a healthy aorta for modeling an AAA. They realized, however, that in a medical image-based model, initial prescription of material and geometric

* Corresponding author at: Department of Mechanical Engineering, 2457 Engineering Building, Michigan State University, East Lansing, MI 48824-1226, United States. Tel.: +1 517 432 3161.
E-mail address: sbaek@egr.msu.edu (S. Baek).

0093-6413/$ – see front matter © 2012 Elsevier Ltd. All rights reserved.
doi:10.1016/j.mechrescom.2012.01.008

properties to satisfy mechanical homeostasis causes the geometry under *in vivo* pressure to deviate from its original geometry obtained from the medical images. To resolve this issue, they employed an optimization method to minimize the deviation of the geometry from the original geometry while maintaining the homeostatic condition (Zeinali-Davarani et al., 2011b). Most recently, the utilities of the G&R model have been illustrated in studying the effect of hemodynamic factors on AAA growth (Sheidaei et al., 2011) and vascular remodeling after endovascular repair (Kwon et al., 2011).

This study summarizes the recent progresses on image-based modeling of AAA growth and presents the most recent framework for modeling AAA G&R, as an important step toward individual-based clinical applications. Using the computational framework and a 3D geometry constructed from medical images of a healthy aorta, we then investigate how the different spatio-temporal distributions of elastin damage and kinetic factors influence local AAA expansion and stress distributions during the progression. Finally, we discuss possible applications of the proposed framework in management of individual AAA patients.

2. A framework for medical image-based modeling of AAA G&R

Fig. 1 illustrates a schematic diagram of a computational framework for modeling AAA enlargement. First, a 3D geometric model is constructed by segmentation of medical images of a healthy aorta. For the aneurysm simulation, we use a central region of the geometric model. Considering the vessel wall as a thin membrane, it is convenient to parameterize the 3D wall surface with two spatial parameters. That is, any point on the wall surface can be characterized by its longitudinal position (l) along the centerline of the artery as well as its azimuthal orientation (θ) with respect to a reference direction (see the 2D plot in Fig. 1 and Zeinali-Davarani et al., 2011b for technical details of the parameterization).

In a normal physiological condition, production and removal of the vascular wall constituents are balanced such that the vessel maintains its shape under a preferred homeostatic state (Humphrey and Rajagopal, 2002). In this computational framework (Fig. 1), we use the geometry constructed from the medical images as the pre-stressed reference configuration. Under the physiological pressure, however, changes in mechanical properties or wall thickness of the computational model of the aorta induce a deviation of the configuration from the original and it is not a trivial task to prescribe the distribution of material and geometric parameters to satisfy the homeostatic mechanical state as well as maintaining the original geometry. Here, we employ a recently proposed inverse optimization to estimate spatial distributions of material and geometric properties, e.g. wall thickness and anisotropy, such that a target mechanical homeostasis is satisfied and the *in vivo* geometry is maintained under *in vivo* condition (Zeinali-Davarani et al., 2011a,b). The general form of the optimization objective function is given as

$$\mathcal{J} = \int_\Omega ||\mathbf{u}(h, \alpha^k) - \mathbf{u}_{image}||^2 dA + \xi \int_\Omega \sum_k \left(\frac{\sigma^k(h, \alpha^k)}{\sigma_h} - 1 \right)^2 dA \tag{1}$$

where $\mathbf{u}$ is the FE solution for displacement field and $\mathbf{u}_{image}$ is the displacement field from the biomedical image. That is $\mathbf{u}_{image} = 0$ when the *in vivo* configuration obtained from the medical image is assumed to be the reference configuration. σ^k is a scalar measure of stress of the constituent k obtained from the FE analysis and σ_h is its homeostatic value. ξ adjusts the minimization weight on each additive term in the objective function. (h, α^k) are the unknown wall thickness and the orientation of the major diagonal fiber family controlling the tissue anisotropy, approximated by

$$h(l, \theta) = \sum_{j=1}^{I} \{\beta_j^h \phi_j(l, \theta)\} \tag{2}$$

$$\alpha^k(l, \theta) = \sum_{j=1}^{I} \{\beta_j^k \phi_j(l, \theta)\}, \tag{3}$$

where (β_j^h, β_j^k) are unknown variables associated with their base functions, $\phi_j(l, \theta)$, which are defined on the 2D computational domain. A direct search method (Nelder-Mead Simplex) is used to estimate spatial distributions of thickness and collagen fiber orientation that minimize the objective function.

Finally, G&R simulations are triggered by inducing damage/degradation to elastin with different spatial and temporal distributions as[1]

$$\mathcal{R}(\mathbf{X}, t) = \mathcal{R}(l, \theta, t) = \mathcal{R}_s(l, \theta)\mathcal{R}_t(t), \tag{4}$$

where the damage ratio, $\mathcal{R} \in [0, 1]$, is the ratio of the degenerated elastin mass to the initial mass.

3. Computational simulation of an AAA evolution

3.1. Kinematics and constitutive relations

Following the previous studies (Baek et al., 2006; Zeinali-Davarani et al., 2011c), consider an aortic wall tissue consisting of multiple structural components, i.e. elastin ($i = e$), four collagen families ($k = 1, \ldots, 4$), and SM cells ($i = m$). We use t for the time associated with the cardiac cycle and s for the time during G&R (Figueroa et al., 2009). The current (*in vivo* quasistatic) configuration κ_s in the G&R timescale is defined as the configuration under the mean (static) pressure during the cardiac cycle (Fig. 2). The configurations κ_τ trace the *in vivo* configurations of body through the time $\tau \in [0, s]$. We assume that each constituent is pre-stretched when deposited into the tissue at time τ and the tensor $\mathbf{G}^i(\tau)$ represents the deposition stretch of constituent i. We consider the prestressed reference configuration (for the computational purpose), κ_R, to be the same as the *in vivo* configuration of the healthy aorta. Furthermore, we assume that particles are created or removed in κ_R so that there is one-to-one mapping between κ_R and κ_s at time s and the total mass is preserved in the mapping between the two configurations. The deformation gradient $\mathbf{F}(s)$ is given corresponding to the mapping from the computational reference κ_R to the current configuration κ_s. Then, the deformation gradient for each constituent i at time t, relative to its natural configuration, $\mathbf{F}^i_{n(\tau)}(t)$, is given by Baek et al. (2006)

$$\mathbf{F}^i_{n(\tau)}(t) = \mathbf{F}(t)\mathbf{F}^{-1}(\tau)\mathbf{G}^i(\tau), \tag{5}$$

where $\mathbf{F}^{-1}(\tau)\mathbf{G}^i(\tau)$ is the tensor representing the pre-stretch of the constituent i that has been produced at τ with respect to the reference configuration.

We employ a hyperelastic model to characterize the mechanical behavior of arterial wall and solve the quasistatic inflation problem

[1] Elastin has been widely observed to be deficient in ruptured and unruptured AAAs. Even though the factors that trigger AAA G&R have not been completely identified yet, elastin degeneration is considered the pathologic factor contributing to the growth of AAAs in this study.

Please cite this article in press as: Zeinali-Davarani, S., Baek, S., Medical image-based simulation of abdominal aortic aneurysm growth. Mech. Re. Commun. (2012), doi:10.1016/j.mechrescom.2012.01.008

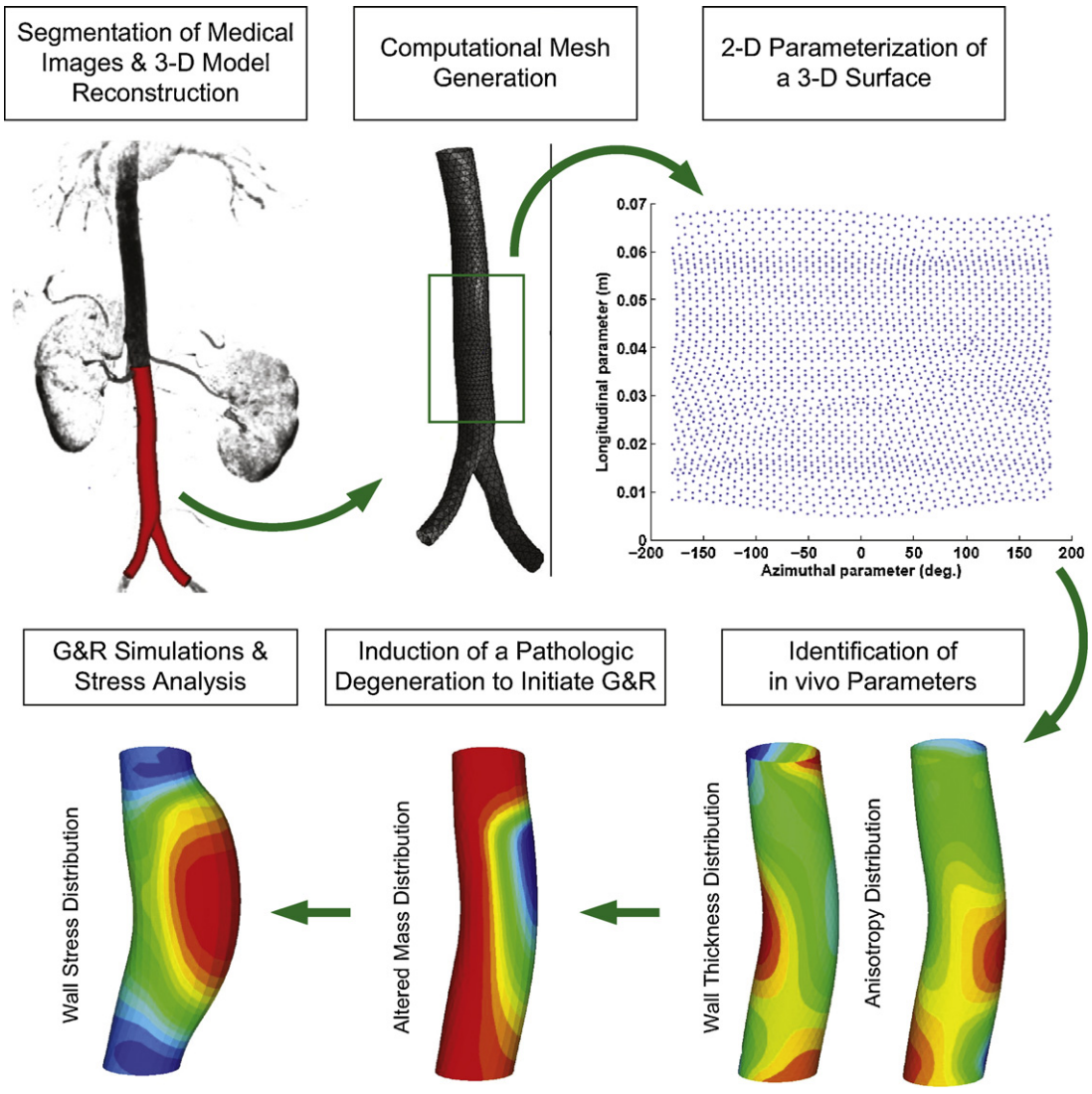

Fig. 1. Schematic diagram of the steps taken for simulating AAAs using a medical image-based geometry and material parameters of a healthy aorta as an initial state.

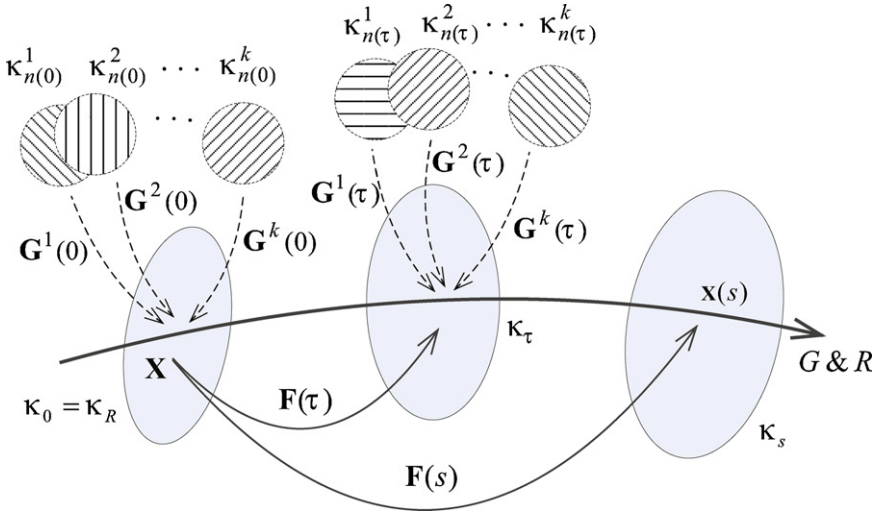

Fig. 2. Schematic view of the configurations involved in G&R simulation. A fixed (prestressed) reference configuration is used for the computation of deformation associated with G&R time $\tau = [0, s]$ and it is chosen to coincide with the configuration of a healthy *in vivo* artery at time ($\tau = 0$).

Please cite this article in press as: Zeinali-Davarani, S., Baek, S., Medical image-based simulation of abdominal aortic aneurysm growth. Mech. Re. Commun. (2012), doi:10.1016/j.mechrescom.2012.01.008

using the principle of virtual work. Then the Cauchy stress can be given as

$$\mathbf{t}(t) = \frac{2}{J(t)}\mathbf{F}(t)\frac{\partial \rho_R(s)\hat{\Psi}(\mathbf{C}(t))}{\partial \mathbf{C}(t)}\mathbf{F}^T(t), \tag{6}$$

where $\hat{\Psi}(\mathbf{C}(t))$ is the stored-energy function (per unit mass). $\rho_R(s) = J(s)\rho(s)$ is the density with respect to the reference configuration where $J(s) = \det[\mathbf{F}(s)]$ and $\rho(s)$ is the mass density in the current configuration at time s. For a membrane model, using $J = J_{2D}h/h_R$ and $\mathbf{T} = h\mathbf{t}$ for the thickness h, the membrane stress $\mathbf{T}$ can be given as

$$\mathbf{T}(t) = \frac{2}{J_{2D}(t)}\mathbf{F}_{2D}(t)\frac{\partial M_R(s)\tilde{\Psi}(\mathbf{C}_{2D}(t))}{\partial \mathbf{C}_{2D}(t)}\mathbf{F}_{2D}^T(t), \tag{7}$$

where the areal density $M_R(s) = h_R\rho_R(s)$ and $\tilde{\Psi}(\mathbf{C}_{2D}(t)) = \hat{\Psi}(\mathbf{C}(t))$. For simplicity, we omit the subscript '2D' and define $w_R(s) = M_R(s)\tilde{\Psi}(\mathbf{C}(t))$. Then (7) becomes

$$\mathbf{T}(t) = \frac{2}{J(t)}\mathbf{F}(t)\frac{\partial w_R(\mathbf{C}(t))}{\partial \mathbf{C}(t)}\mathbf{F}^T(t). \tag{8}$$

To simulate arterial G&R, we postulate the stored energy equation $w_R(t;s)$ to be (Figueroa et al., 2009; Zeinali-Davarani et al., 2011c)

$$w_R(t;s) = \sum_i \{M_R^i(0)Q^i(s)\Psi^i(\mathbf{C}^i_{n(0)}(t)) + \int_0^s m_R^i(\tau)q^i(s,\tau)\Psi^i(\mathbf{C}^i_{n(\tau)}(t))d\tau\}, \tag{9}$$

where $\Psi^i(\mathbf{C}^i_{n(\tau)}(t))$ is the stored energy of constituent i that has been produced at time τ, $\mathbf{C}^i_{n(\tau)}(t) = [\mathbf{F}^i_{n(\tau)}(t)]^T\mathbf{F}^i_{n(\tau)}(t)$, $Q^i(s)$ is the fraction of the constituent i that was present at time 0 and still remains at time s (i.e. has not been yet removed), $m_R^i(\tau)$ is the mass production rate of the constituent i at time τ per unit reference area, and $q^i(s,\tau)$ is its survival function, that is, the fraction of the constituent that has been produced at time τ and remains at time s.

The strain energy functions for the elastin-dominated amorphous, collagen fiber families ($\Psi^k = \Psi^c$) and passive SM are given as

$$\Psi^e(\mathbf{C}_n^e(t)) = \frac{c_1}{2}\left(C^e_{n[11]} + C^e_{n[22]} + \frac{1}{C^e_{n[11]}C^e_{n[22]} - {C^e_{n[12]}}^2} - 3\right), \tag{10}$$

$$\Psi^c(\lambda^k_{n(\tau)}(t)) = \frac{c_2}{4c_3}\left\{\exp[c_3(\lambda^k_{n(\tau)}(t)^2 - 1)^2] - 1\right\}, \tag{11}$$

$$\Psi^m(\lambda^m_{n(\tau)}(t)) = \frac{c_4}{4c_5}\left\{\exp[c_5(\lambda^m_{n(\tau)}(t)^2 - 1)^2] - 1\right\}, \tag{12}$$

where

$$\lambda^k_{n(\tau)}(t) = G_h^c\frac{\lambda^k(t)}{\lambda^k(\tau)}, \quad \lambda^k(t) = \sqrt{\mathbf{F}(t)\mathbf{M}^k(\tau)\cdot\mathbf{F}(t)\mathbf{M}^k(\tau)}, \tag{13}$$

$\mathbf{M}^k(\tau)$ is the unit vector in the direction of collagen fiber family k in κ_R, and $C^e_{n[11]}$, $C^e_{n[22]}$ and $C^e_{n[12]}$ are components of $\mathbf{C}_n^e = [\mathbf{F}_n^e]^T\mathbf{F}_n^e$. Vascular SM cells have active tone *in vivo* and the level of contraction can vary under physiological and pathological conditions. We use a potential function for active tone as (Zulliger et al., 2004; Baek et al., 2007)

$$\Psi^m_{act}(t) = \frac{S}{\rho}\left\{\lambda^m_{act}(t) + \frac{1}{3}\frac{(\lambda_M - \lambda^m_{act}(t))^3}{(\lambda_M - \lambda_o)^2}\right\}, \tag{14}$$

where λ_M and λ_o are stretches at which the active force generation is maximum and zero, $\lambda^m_{act}(t)$ is the stretch of the SM in circumferential direction at time t, and S is the stress at the maximum contraction. The vasoactive response can shift via rearrangement of SM cells (Baek et al., 2007). In this model, we assume that the vasoactive response changes with G&R during the progression of an AAA so that the intermediate configuration κ_s is considered as the reference for the vasoactive response. Hence, here $\lambda^m_{act}(t)$ is calculated as the circumferential stretch during the cardiac cycle from κ_s. Then, the total membrane strain energy becomes $w_R = w_{R(passive)} + M_R^m(t)\Psi^m_{act}$.

3.2. G&R mediated by stress

Production and removal of constituents in vascular tissues are continuous processes and the tissue mass and its configuration are maintained by balanced turnover of constituents. The rates of production and removal changes from their balanced normal (basal) values in response to changes in mechanical environment. Here, we assume that $m_R^e(s) = 0$ and the rates of mass production for collagen fibers and SM are functions of a scalar measure of intramural stress, given by

$$m_R^k(s) = \frac{M_R^c(s)}{M_R^c(0)}(K_g^c(\boldsymbol{\sigma}^k(s) - \boldsymbol{\sigma}_h^c) + m^k_{basal}) \tag{15}$$

$$m_R^m(s) = \frac{M_R^m(s)}{M_R^m(0)}(K_g^m(\boldsymbol{\sigma}^m(s) - \boldsymbol{\sigma}_h^m) + m^m_{basal}) \tag{16}$$

where $M_R^c(0)$ and $M_R^m(0)$ are the mass of collagen and SM per reference area of a healthy artery at time 0, respectively, K_g^c and K_g^m are sensitivity parameters that control the stress-mediated growth of collagen and SM, m^i_{basal} is a basal rate of mass production for the constituent i, and

$$\boldsymbol{\sigma}^k(s) = \frac{\left\|\mathbf{T}^c(s)\mathbf{m}^k(s)\right\|}{h^c(s)}, \quad \boldsymbol{\sigma}^m(s) = \frac{\left\|\mathbf{T}^m(s)\mathbf{m}^m(s)\right\|}{h^m(s)}. \tag{17}$$

where $\mathbf{T}^c(s)$ and $\mathbf{T}^m(s)$ are the Cauchy membrane stress contributed by collagen and SM at time s (i.e. $\mathbf{T}^c(s) = \sum_{k=1}^4\mathbf{T}^k(s)$). $h^c(s)$ and $h^m(s)$ are contributions of collagen and SM to the total thickness at time s. $\mathbf{m}^k(s)$ and $\mathbf{m}^m(s)$ are unit vectors in the direction of the corresponding constituents. Also, let

$$q^i(s,\tau) = \begin{cases} \exp(-\int_\tau^s k_q^i(\tilde{\tau})d\tilde{\tau}) & s - \tau \le a^i_{max} \\ 0 & s - \tau > a^i_{max} \end{cases}, \tag{18}$$

where $k_q^i(\tilde{\tau})$ is a rate parameter for removal of constituent i, and a^i_{max} is the maximum life span of the constituent i.

We assume that the alignment of the newly produced collagen is influenced by the orientation of the existing collagen and it consequently aligns along the direction of the existing collagen family (Baek et al., 2006).

3.3. Finite element formulation

Assuming the arterial wall as the membrane, the weak form is derived from the principle of virtual work as

$$\delta I = \int_S \delta w_R dA - \int_s P\mathbf{n}\cdot\delta\mathbf{x}da = 0, \tag{19}$$

where P is the transmural pressure and $\mathbf{n}$ is the outward normal unit vector. Let the finite approximation of the current position $\mathbf{x}$ be given as

$$\mathbf{x} = \boldsymbol{\Phi}\mathbf{x}^p, \quad x_i = \Phi_{iA}x_A^p, \tag{20}$$

Please cite this article in press as: Zeinali-Davarani, S., Baek, S., Medical image-based simulation of abdominal aortic aneurysm growth. Mech. Re. Commun. (2012), doi:10.1016/j.mechrescom.2012.01.008

Table 1
Simulation case description.

Cases 1–6:	$\mathcal{R} = \mathcal{R}_s(l,\theta), K_g^i = 0.05$
Case 7:	$\mathcal{R} = \mathcal{R}_s(l,\theta), K_g^i = K_g^i(l,\theta)$
Case 8:	$\mathcal{R} = \mathcal{R}(l,\theta,t), K_g^i = K_g^i(\mathcal{R}(l,\theta,t))$

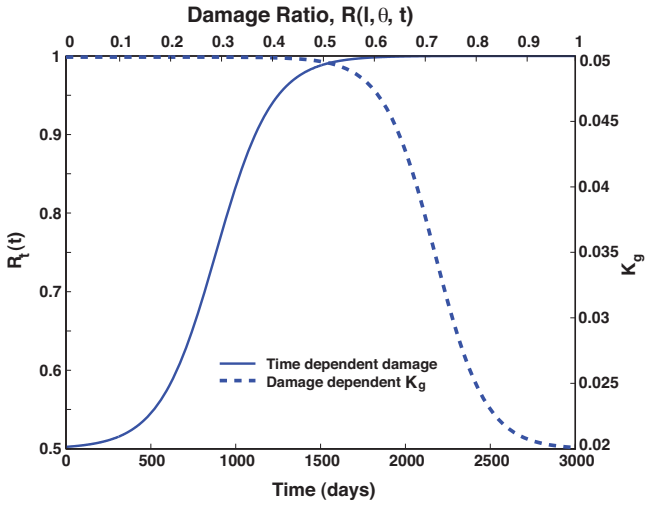

Fig. 3. Variation of damage ratio with respect to time ($\mathcal{R}_t$ vs. time) and variation of the sensitivity parameter with respect to the local damage (K_g vs. $\mathcal{R}(l,\theta,t)$).

where $\mathbf{x}^p$ and $\boldsymbol{\Phi}$ are the nodal vector for the current position and shape function matrix, respectively. The governing equations for an element are derived from the weak form as

$$\{\mathcal{F}\}_P^e = \int_{S^e} \left(\frac{\partial w_R}{\partial C_{\alpha\beta}} \frac{\partial C_{\alpha\beta}}{\partial x_P^p} - \tilde{P}_i \Phi_{iP} \right) dA = 0, \tag{21}$$

where $C_{\alpha\beta}$ are components of 2D right Cauchy–Green deformation tensor. Finally, Eq. (21) is solved for $\mathbf{x}^p$ by the Newton–Raphson method. More details of the G&R model and the FE formation can be found in Zeinali-Davarani et al. (2011c).

3.4. AAA simulation cases

Table 1 briefly describes all the simulation cases. In the first set of simulations, to study the effect of spatial variation of elastin degradation, AAAs are initiated by inducing instantaneous degradation with multiple (six) spatial shapes considering a uniform value of the G&R kinetic parameter (Cases 1–6). To study the role of kinetic parameter, in Case 7, AAA growth simulation is repeated with spatially uniform kinetic parameter ($K_g^i = 0.05$) and non-uniform distribution of the kinetic parameter (a reduced value at the aneurysm sac; $K_g^i = 0.02$). In Case 8, the elastin degradation is assumed to be a function of time as well as the location and K_g^i is assumed to depend on the local damage at a given time (see Fig. 3).

4. Results

Fig. 4 shows a set of distinct shapes of spatial damage (distributions of elastin areal mass density) and the resulting AAAs with the corresponding von Mises stress distributions. The time histories of the variations of the peak von Mises stress during enlargement of 5 aneurysms are plotted in Fig. 5a. Evidently, inducing damage is followed by a sharp increase in the peak stress (on the regions that match with the maximum degradation) which, after a time delay, begins to gradually diminish via stress-mediated collagen turnover. The decline of peak stress is initially sharper but becomes slower during the AAA expansion. In some cases the stress increases again after some time (e.g. around 4 years) on the regions where the extent of degradation was not necessarily maximal (see regions specified by black arrows in Fig. 4). The maximum diameter of aneurysms changes linearly over time but at different rates depending on the damage shape (Fig. 5b).

Fig. 6 depicts spatial correlations between von Mises stress and both the rate of mass production and the rate of nodal displacement for Cases 1 and 5. The maximum rates of mass production and displacement gradually increase with aneurysm expansion while the peak stress reduces. In general, the rate of mass production increases with the stress, but regions of high stress correspond to a wider range of mass production and displacement rates especially in advanced stages.

In a different simulation case (Case 7), an aneurysm is generated with a uniform value of K_g^i (Fig. 7a) as well as spatially varying K_g^i (Fig. 7b). Simulation with a lower value of the kinetic parameter (i.e. $K_g = 0.02$) on the region where aneurysm sac forms leads to lower rates of the local mass production and faster enlargement. Insufficient local mass production also leads to an increase of the local wall stress during enlargement (Fig. 7b).

Fig. 8 shows the distributions of elastin and collagen areal mass density and the von Mises stress for Case 8 where the elastin damage is time-dependent and K_g is assumed to be damage-dependent (relations shown in Fig. 3). Increasing degradation along with gradually decreasing K_g accelerate the AAA enlargement and heightens wall stress (up to 450 kPa).

5. Discussion

This study summarized our recent effort to provide a framework for developing medical image-based models of AAAs considering multiple spatio-temporal forms of elastin degradation and stress-mediated collagen turnover. The computational framework included the identification of material/geometric parameters as a key step before G&R simulation and diverse simulation cases, facilitated by 2D parameterization of the wall surface. Our computational simulation of AAAs were not yet specific to an AAA patient in the sense that it did not use the medical images from an AAA patient but used images from a healthy subject. Nevertheless, the same computational framework could be used in a patient-specific modeling of an AAA with a better understanding of mechanical homeostasis under pathological conditions. The simulation results also captured some general characteristics of AAA expansion such as linear trend of expansion over time. Some of the simulated shapes of AAAs were comparable to images of real AAAs. For example Cases 1 and 2 provided general shapes similar to cases studied by Raghavan et al. (2000). Collagen content was markedly increased during G&R consistent with histological observations (Menashi et al., 1987). We also noticed an increase in anisotropy in circumferential direction, consistent with observations by Vande Geest et al. (2006).

The high stress regions arisen during intermediate stages of AAA growth in Cases 1 and 5 (Fig. 4) were found to be consistent with stress analysis using patient-specific models in other FE studies (Vorp et al., 1998; Scotti et al., 2005; Doyle et al., 2010; Hua and Mower, 2001; Giannoglou et al., 2006), confirming the regions of inflections as the high stress regions. We noticed a strong spatial correlation between the rate of collagen production and wall stress in earlier stage of growth. Later, even though the peak wall stress was reduced, collagen was still produced at an increased rate (Fig. 6). This seems to be mainly because the rate of mass production is linearly related to the number of cells (or the collagen mass in Eq. (15)) at a given time. There was a strong spatial correlation between damage and the rate of mass production at all times (not shown), whereas a weaker correlation was found between the local

Please cite this article in press as: Zeinali-Davarani, S., Baek, S., Medical image-based simulation of abdominal aortic aneurysm growth. Mech. Re. Commun. (2012), doi:10.1016/j.mechrescom.2012.01.008

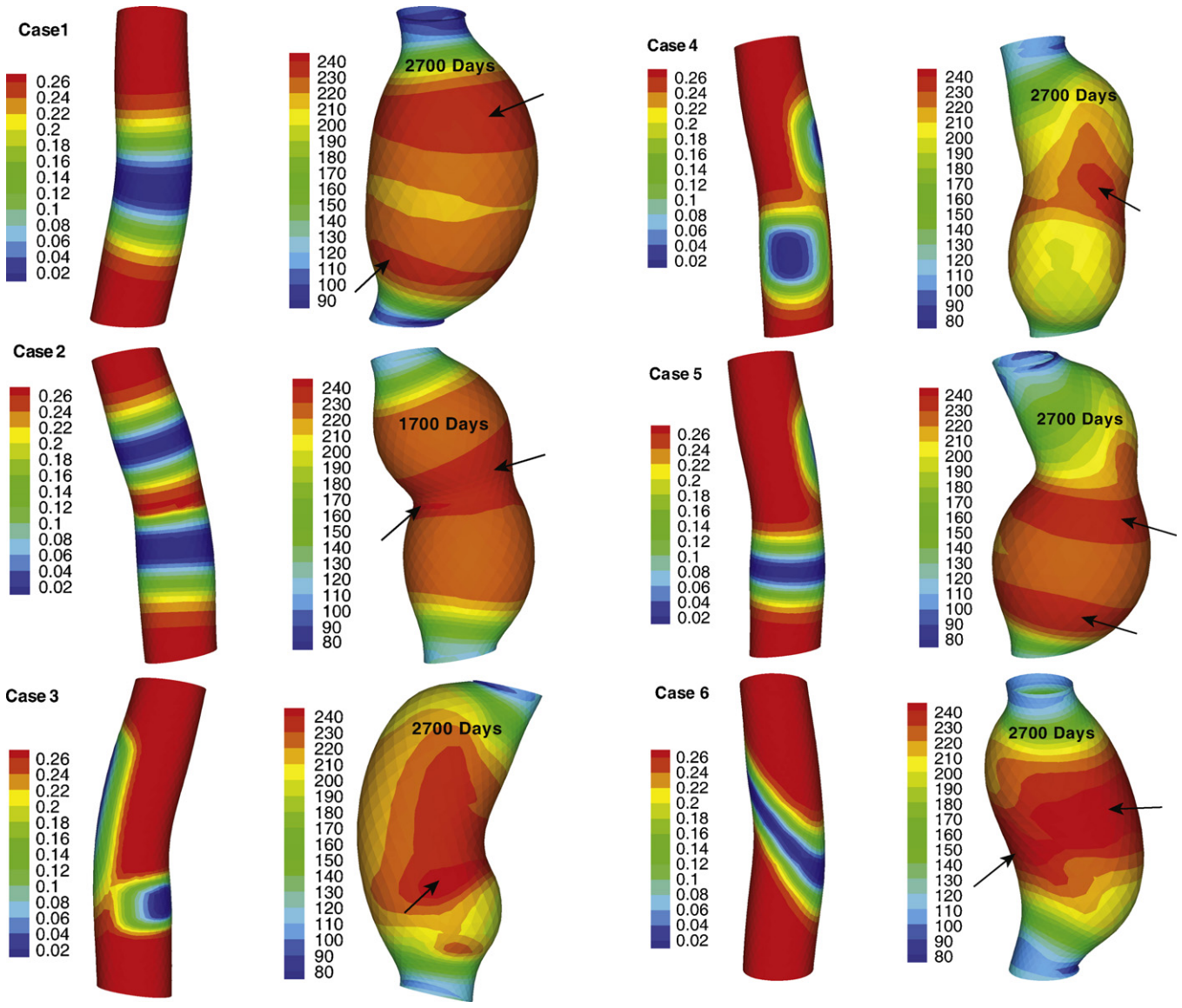

Fig. 4. Left: Areal mass distributions (kg/m^2) of elastin after introducing damage. Right: The shapes of AAAs after the G&R simulation and distributions of von Mises stress (kPa). The arrows indicate the regions of elevated stress during AAA expansion.

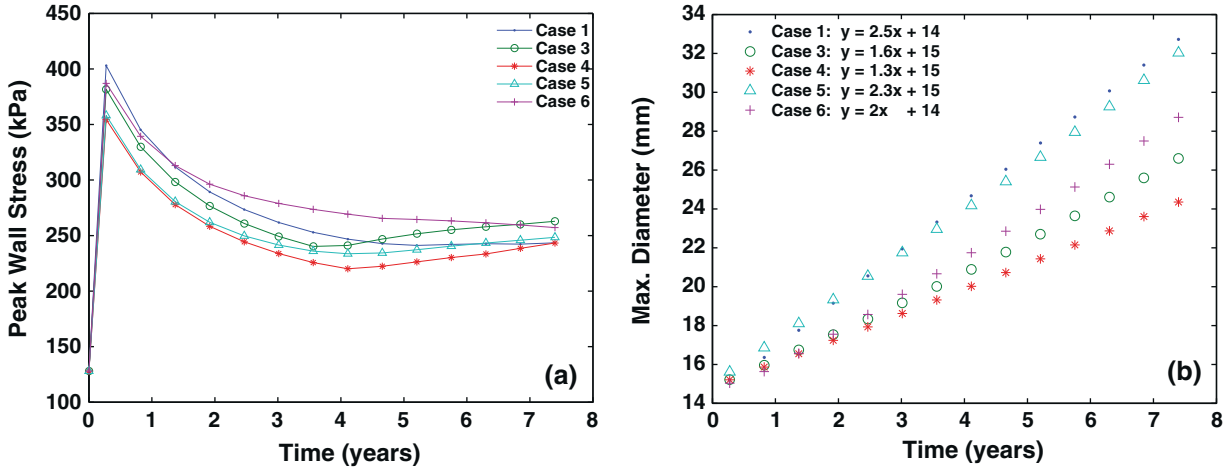

Fig. 5. Variations of peak von Mises stress (a) and maximum diameter (b) with G&R time for different cases. Equations for best fit lines are shown (lines are not included in the graph).

Please cite this article in press as: Zeinali-Davarani, S., Baek, S., Medical image-based simulation of abdominal aortic aneurysm growth. Mech. Re. Commun. (2012), doi:10.1016/j.mechrescom.2012.01.008

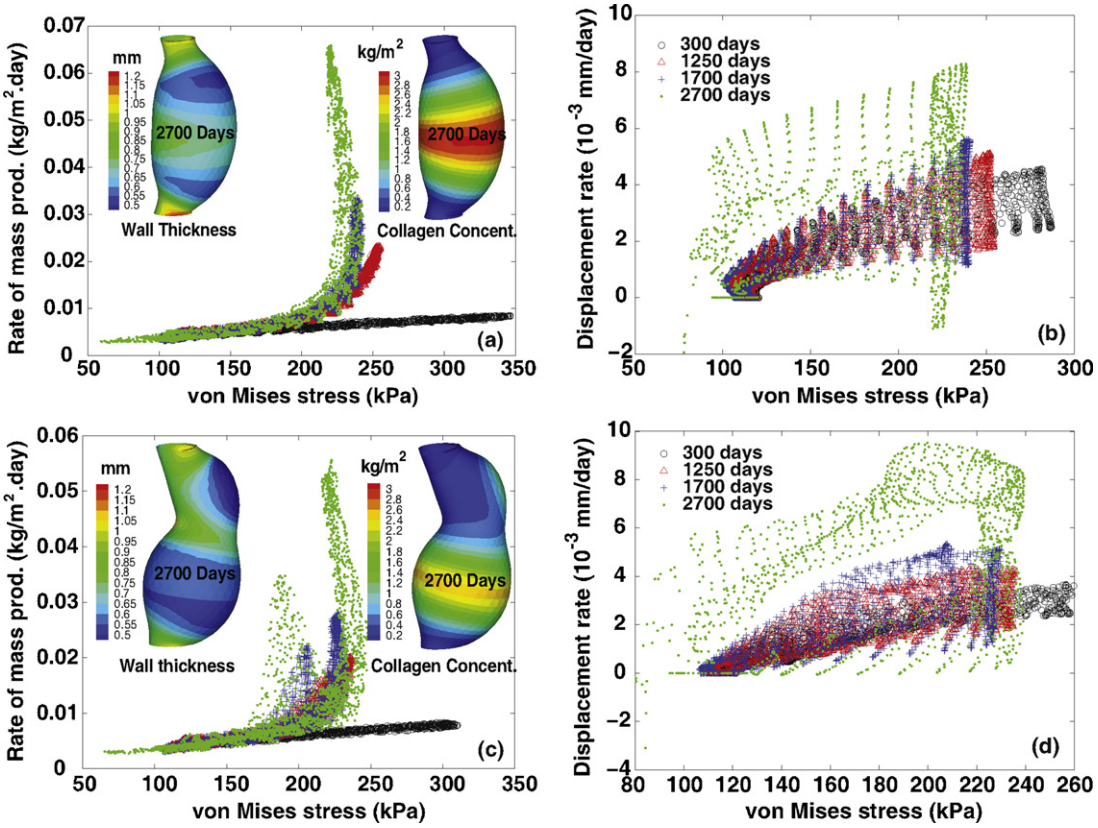

Fig. 6. Spatial relations between von Mises stress and both the rate of collagen mass production as well as the rate of wall displacement for Cases 1 and 5 at different stages of growth. Wall thickness distribution and collagen concentration are illustrated for each case corresponding to 2700 days of G&R.

damage and wall displacement in advanced AAAs (Fig. 9). In Case 1, wall displacement occurred globally and was not restricted to the damaged regions, while in Case 3 high wall displacement was more confined to the damaged regions (Fig. 9). Interestingly, in Case 1, although the damage was uniformly distributed around the circumference (Fig. 4), the lesion on the convex side results in more displacement than the concave side (see Figs. 4 and 9).

While higher values of K_g could stabilize the aneurysm enlargement (Zeinali-Davarani et al., 2011c), lower values reduced the sensitivity of the stress-mediated mechanism and resulted in an increase in the peak wall stress (on regions with lower sensitivity) and a higher rate of expansion (Fig. 7). Inherent variability in the sensitivity of stress-mediated G&R among individuals (due to genetic factors or individual life-style) may partly explain the variability of collagen content observed among different AAAs (Ghorpade and Baxter, 1996; Rizzo et al., 1989; Sumner et al., 1970).

The time-dependent case (Case 8) was inspired by a possibility of increasing elastin degradation due to exacerbated hemodynamic conditions in AAAs as the geometry evolves (Mohan et al., 1999; Walpola et al., 1993). Recently Sheidaei et al. (2011) demonstrated the effect of low wall shear stress on elastin degradation and acceleration of the an AAA expansion through coupling with hemodynamic simulation. However, wall shear stress seems to play more complex roles in pathogenesis of AAAs. Low wall shear stress

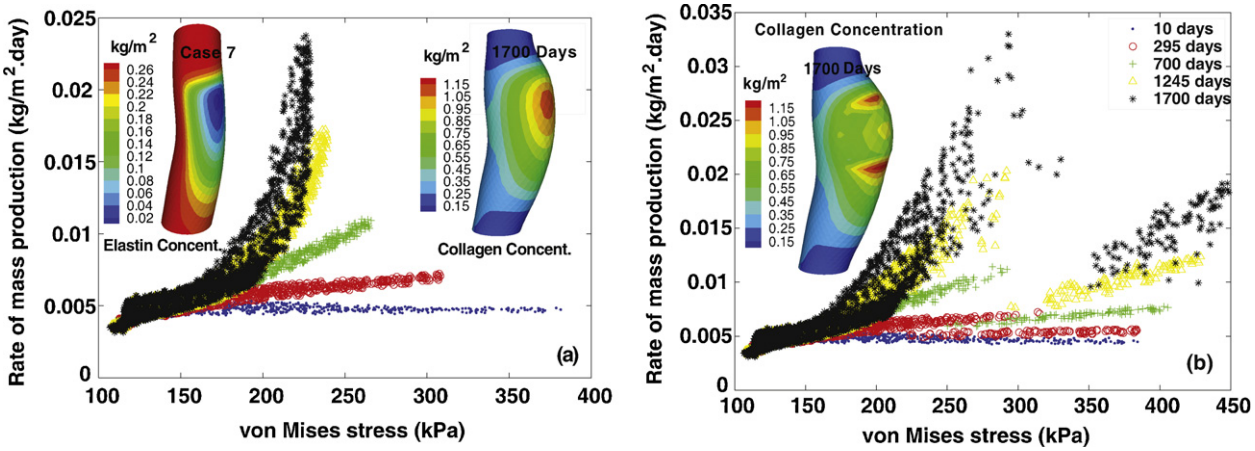

Fig. 7. Spatial relation between the rate of collagen mass production and von Mises stress for Case 7 using a homogeneous distribution of kinetic parameters (a; $K_g = 0.05$) as well as spatially variable kinetic parameter (b; $K_g = 0.02$ at the AAA sac and $K_g = 0.05$ otherwise) at different times.

Please cite this article in press as: Zeinali-Davarani, S., Baek, S., Medical image-based simulation of abdominal aortic aneurysm growth. Mech. Re. Commun. (2012), doi:10.1016/j.mechrescom.2012.01.008

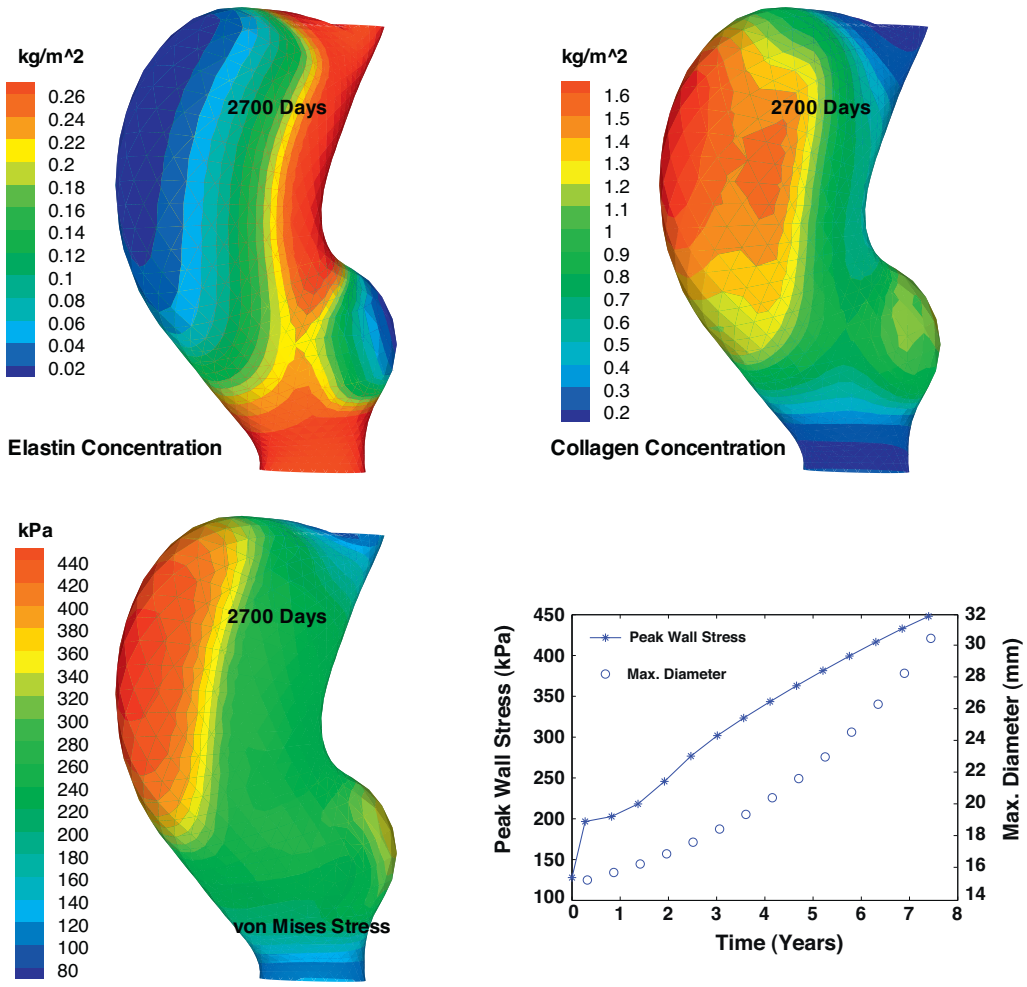

Fig. 8. Elastin and collagen mass areal density along with von Mises stress distributions for Case 8 after 7 years (2700 days) of G&R. Time history of maximum diameter and peak von Mises stress is shown.

promotes collagen production as well (Malek and Izumo, 1995; Rizvi et al., 1996). Wall shear stress may be a key mediator of AAA G&R that should be included in the growth laws as more information becomes available for the underlying kinetics. In addition, the dependence of K_g^i on the extent of elastin damage (damage-induced weakening of the G&R sensitivity) was considered because the loss of elastin is associated with SM migration or proliferation (Karnik et al., 2003; Li et al., 1998), apoptosis (Lopez-Candales et al., 1997; Thompson et al., 1997) and its phenotype modulation (Ailawadi et al., 2009). It may be possible, then, to hypothesize that elastin

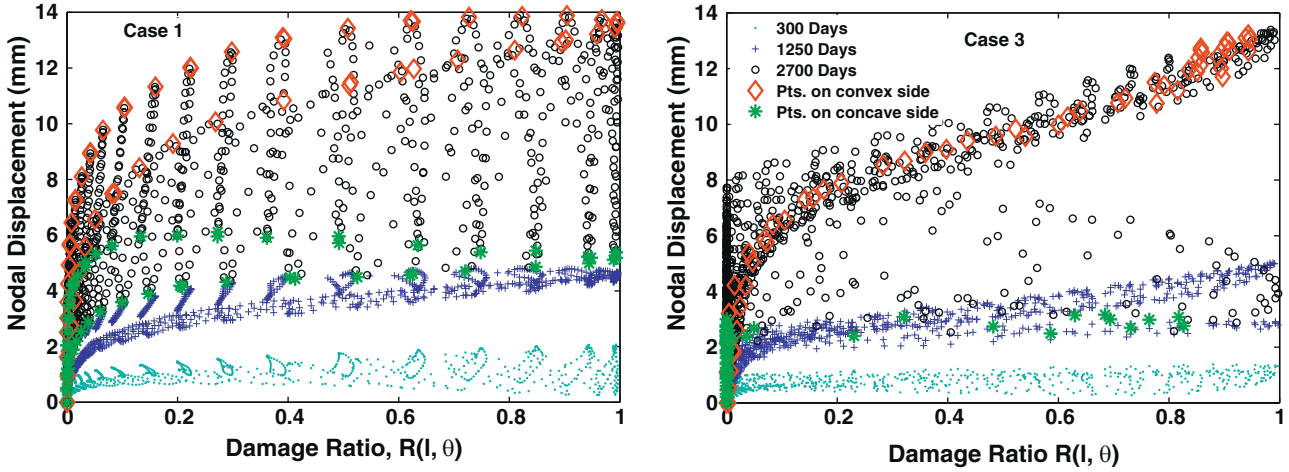

Fig. 9. Spatial relation between the nodal displacement and the damage ratio for Cases 1 and 3 at different times. A number of points on the convex and concave regions (with reference to the healthy geometry) are distinguished with different markers at 2700 days.

Please cite this article in press as: Zeinali-Davarani, S., Baek, S., Medical image-based simulation of abdominal aortic aneurysm growth. Mech. Re. Commun. (2012), doi:10.1016/j.mechrescom.2012.01.008

degradation compromises the compensatory mass production via diminished SM cells. The imbalance between extracellular matrix synthesis (Sumpio et al., 1988) and degradation (Crowther et al., 2000), mediated by altered SM cells can be the reason for progressive weakening and rupture of the wall. Recently, Maier et al. (in press) have quantitatively found a spatial correlation between wall stress and the level of *in vivo* tissue reactions which can indicate either synthetic or proteolytic activities in the arterial wall tissue.

In this study, we were able to capture relatively complex 3D shapes of AAAs by prescribing distinct shapes for spatial damages. Even with a fixed spatial distribution of elastin damage, we noticed that regions of elevated wall stress can change in the course of expansion (Fig. 4). Interestingly, during the evolution of some AAA shapes, the peak wall stress locally increased again (Fig. 5). The lesions in Cases 1 and 5 develop lower peak wall stress than those in Cases 3 and 6 even with larger diameter after 7 years, implying the influence of local aneurysm shape on the peak wall stress, beyond what the maximum diameter criterion may solely suggest.

Together, these results emphasize the impact of geometrical complexities on stress distributions during AAA expansion as suggested by Sacks et al. (1999). Other studies have sought correlations between wall stress and quantified AAA shapes, asymmetry, tortuosity, as alternative indicators of rupture (Shum et al., 2011; Vorp et al., 1998; Georgakarakos et al., 2010; Doyle et al., 2009; Giannoglou et al., 2006). Moreover, we found that the regions of low wall thickness initially coincide with the damaged regions but they too change as the lesions evolve. In some cases they may correspond to high stress regions (e.g. Cases 1 and 5; Figs. 4 and 6) while in other cases they may not (other cases not shown). Coincidence of the low wall thickness and elevated wall stress could be indicative of an impending rupture in advanced stages. An advantage of G&R simulations is that it can capture morphological complexities during enlargement as well as the evolution of wall properties during G&R.

AAAs are often accompanied by bending of the proximal neck area which influences the hemodynamics and possibly intraluminal thrombus formation (Biasetti et al., 2010). Fig. 10 depicts the axial stretch distributions for different simulation cases. Aneurysms enlarge in both circumferential and axial directions and because of the fixed boundary condition, axial stretch on the neck region reduces to values less than 1. Even if not the main reason, this can be used as an indicator of where bending may occur in later stages (Jackson et al., 2005). This is consistent with Watton et al. (2004) who found minimum axial stress close to proximal and distal ends of their AAA models. It is noteworthy that we have modeled the vessel wall as a membrane while a model that accounts for bending of the wall is necessary to study buckling of the vessel walls. A full 3D model will also facilitate distinction between layers

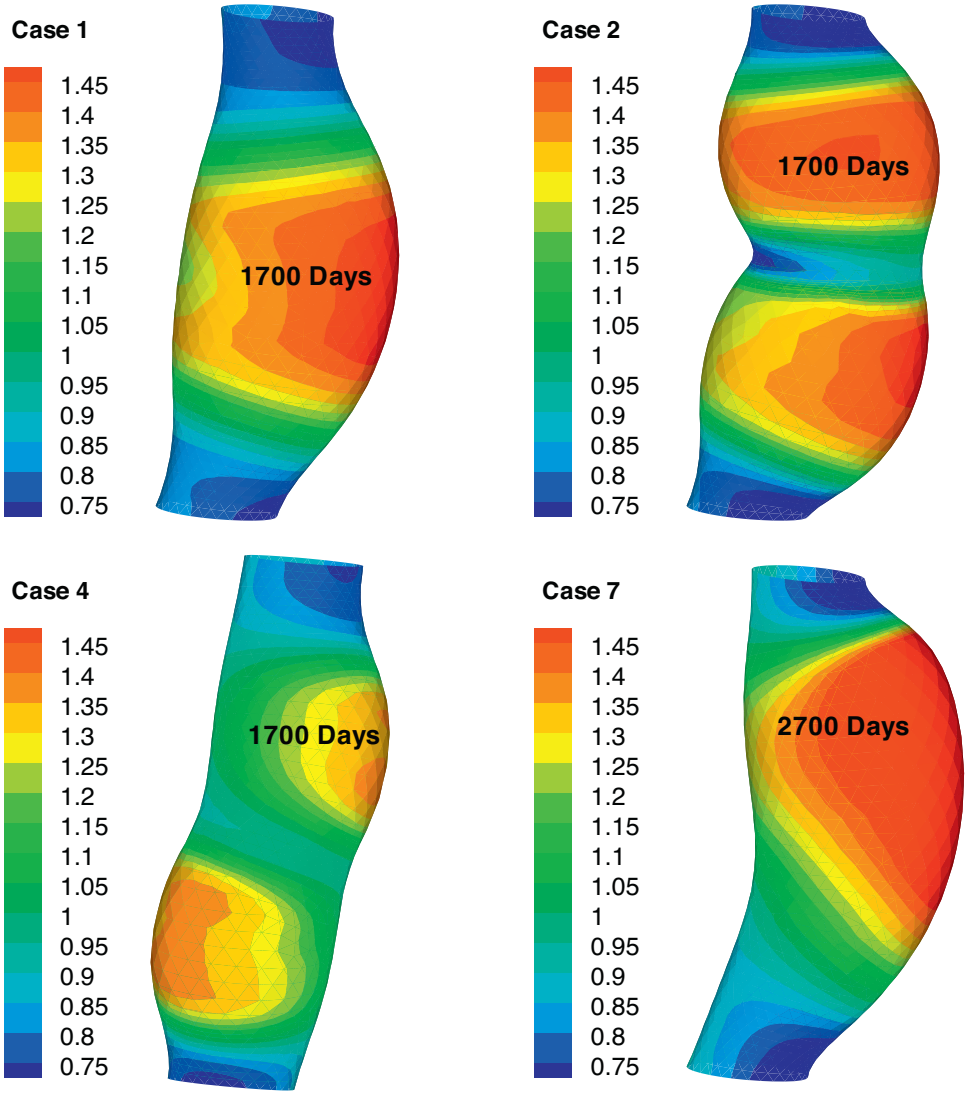

Fig. 10. Distributions of axial stretch for different aneurysms.

Please cite this article in press as: Zeinali-Davarani, S., Baek, S., Medical image-based simulation of abdominal aortic aneurysm growth. Mech. Re. Commun. (2012), doi:10.1016/j.mechrescom.2012.01.008

of wall and distribution of constituents and parameters through the thickness.

From the practical point of view, we are ultimately interested in modeling AAA expansion from an existing AAA, which is an intermediate stage of the disease. While the current model uses the assumption of homeostatic condition for the healthy aorta to prescribe initial conditions (e.g. thickness, fiber alignment, kinetic parameters) of the simulation, less information is available for the spatial and temporal distribution of the parameters for a diseased artery. Despite this challenge, we believe that the current model can be used for estimating the material and kinetic parameters of an existing AAA and, hence, predicting patient-specific AAA expansion if used in a broader framework. For example, using the same model but in an inverse scheme, it seems feasible to regenerate a patient-specific AAA shape by estimating spatio-temporal distributions of elastin degradation as well as the G&R sensitivity/kinetic parameter. Cyclic strain quantified from medical images can also be incorporated into the inverse scheme such that the local mechanical state of the AAA can be more accurately predicted. That would also require further enhancement of the computational model regarding boundary conditions, e.g. the spine support, which is an ongoing study by our group. Our preliminary study shows that including the spine as a growth barrier in the G&R model significantly alters the resulting AAA shape and stress/cyclic strain distributions.

There is still lack of verification for the estimated distributions of the wall thickness and fiber orientation in healthy condition (prior to G&R) and during the AAA development for the current study. Recent advances in medical imaging and segmentation techniques make it possible to quantify *in vivo* wall thickness (Shum et al., 2010; Martufi et al., 2009) and it will allow for the verification of the patient-specific simulations of AAAs in the future study. A major limitation of the current model is that the role of intraluminal thrombus layer is overlooked. Thrombus has been found to either protect the wall by reducing the wall stress (Inzoli et al., 1993; Thubrikar et al., 2003; Wang et al., 2002) or compromise its integrity via biochemical environment (Vorp et al., 2001; Fontaine et al., 2002).

In conclusion, in this paper we presented a computational framework for modeling AAAs G&R using a geometry constructed from medical images. However toward individual patient-based clinical application, the current framework will require continuous improvement regarding constitutive description of the aortic tissue, boundary conditions, and G&R rules and the development of an inverse scheme using longitudinal medical images from patients.

Acknowledgements

The work was supported in part by the NSF (CMMI-1150376). The authors also acknowledge the support of the Michigan State University High Performance Computing Center and the Institute for Cyber-Enabled Research.

References

Ailawadi, G., Moehle, C.W., Pei, H., Walton, S.P., Yang, Z., Kron, I.L., Lau, C.L., Owens, G.K., 2009. Smooth muscle phenotypic modulation is an early event in aortic aneurysms. J. Thorac. Cardiovasc. Surg. 138, 1392–1399.

Baek, S., Rajagopal, K.R., Humphrey, J.D., 2006. A theoretical model of enlarging intracranial fusiform aneurysms. J. Biomech. Eng. 128, 142–149.

Baek, S., Valentín, A., Humphrey, J.D., 2007. Biochemomechanics of cerebral vasospasm and its resolution: II. Constitutive relations and model simulations. Ann. Biomed. Eng. 35, 1498–1509.

Biasetti, J., Gasser, T., Auer, M., Hedin, U., Labruto, F., 2010. Hemodynamics of the normal aorta compared to fusiform and sacuular abdominal aoritic aneurysms with emphasis on a potential thrombus formation mechanism. Ann. Biomed. Eng. 38, 380–390.

Crowther, M., Goodall, S., Jones, J.L., Bell, P.R., Thompson, M.M., 2000. Increased matrix metalloproteinase 2 expression in vascular smooth muscle cells cultured from abdominal aortic aneurysms. J. Vasc. Surg. 32, 575–583.

Dorfmann, A., Wilson, C., Edgar, E.S., Peatte, R.A., 2010. Evaluating patient-specific abdominal aortic aneurysm wall stress based on flow-induced loading. Biomech. Model. Mechanobiol. 9 (2), 127–139.

Doyle, B.J., Callanan, A., Burke, P.E., Grace, P.A., Walsh, M.T., Vorp, D.A., McGloughlin, T.M., 2009. Vessel asymmetry as an additional diagnostic tool in the assessment of abdominal aortic aneurysms. J. Vasc. Surg. 49, 443–454.

Doyle, B.J., Cloonan, A.J., Walsh, M.T., Vorp, D.A., McGloughlin, T.M., 2010. Identification of rupture locations in patient-specific abdominal aortic aneurysms using experimental and computational techniques. J. Biomech. 43, 1408–1416.

Driss, A.G., Benessiano, J., Poitevin, P., Levy, B.I., Michael, J.-B., 1997. Arterial expansive remodeling induced by high flow rates. Am. J. Physiol. 272 (2), H851–H858.

Figueroa, C.A., Baek, S., Taylor, C.A., Humphrey, J.D., 2009. A computational framework for fluid-solid-growth modeling in cardiovascular simulations. Comput. Methods Appl. Mech. Eng. 198, 3583–3602.

Fillinger, M.F., Raghavan, M.L., Marra, S.P., Cronenwell, J.L., Kennedy, F.E., 2002. In vivo analysis of mechanical wall stress and abdominal aortic aneurysm rupture risk. J. Vasc. Surg. 36 (3), 589–597.

Fontaine, V., Jacob, M.P., Houard, X., Rossignol, P., Plissonnier, D., Angles-Cano, E., Michel, J.B., 2002. Involvement of the mural thrombus as a site of protease release and activation in human aortic aneurysms. Am. J. Pathol. 161 (5), 1701–1710.

Georgakarakos, E., Ioannou, C.V., Kamarianakis, Y., Papaharilaou, Y., Kostas, T., Manousaki, E., Katsamouris, A.N., 2010. The role of geometric parameters in the prediction of abdominal aortic aneurysm wall stress. Eur. J. Vasc. Endovasc. Surg. 39, 42–48.

Ghorpade, A., Baxter, B.T., 1996. Biochemistry and molecular regulation of matrix macromolecules in abdominal aortic aneurysms. Ann. N. Y. Acad. Sci. 800, 138–150.

Giannoglou, G., Giannakoulas, G., Soulis, J., Chatzizisis, Y., Perdikides, T., Melas, N., Parcharidis, G., Louridas, G., 2006. Predicting the risk of rupture of abdominal aortic aneurysms by utilizing various geometrical parameters: Revisiting the diameter criterion. Angiology 57, 487–494.

Hariton, I., deBotton, G., Gasser, T.C., Holzapfel, G.A., 2007. Stress-driven collagen fiber remodeling in arterial walls. Biomech. Model. Mechanobiol. 6, 163–175.

Hua, J., Mower, W.R., 2001. Simple geometric characteristics fail to reliably predict abdominal aortic aneurysm wall stresses. J. Vasc. Surg. 34, 308–315.

Humphrey, J.D., Rajagopal, K.R., 2002. A constrained mixture model for growth and remodeling of soft tissues. Math. Models Methods Appl. Sci. 12, 407–430.

Inzoli, F., Boschetti, F., Zappa, M., Longo, T., Fumero, R., 1993. Biomechanical factors in abdominal aortic aneurysm rupture. Eur. J. Vasc. Surg. 7, 667–674.

Jackson, Z.S., Dajnoweiec, D., Gotlieb, A.I., Langille, B.L., 2005. Partial off-loading of longitudinal tension induces arterial tortuosity. Arterioscler. Thromb. Vasc. Biol. 25 (5), 957–962.

Karnik, S.K., Brooke, B.S., Bayes-Genis, A., Sorensen, L., Wythe, J.D., Schwartz, R.S., Keating, M.T., Li, D.Y., 2003. A critical role for elastin signaling in vascular morphogenesis and disease. Development 130 (2), 411–423.

Kroon, M., Holzapfel, G.A., 2007. A model for saccular cerebral aneurysm growth by collagen fibre remodelling. J. Theor. Biol. 247 (4), 775–787.

Kroon, M., Holzapfel, G.A., 2009. A theoretical model for fibroblast-controlled growth of saccular cerebral aneurysms. J. Theor. Biol. 257 (1), 73–83.

Kwon, S., Rectenwald, J., Baek, S., 2011. Intrasac pressure changes and vascular remodeling after endovascular repair of abdominal aortic aneurysms: Review and biomechanical model simulation. J. Biomech. Eng. 133, 011011.

Li, D.Y., Brooke, B., Davis, E.C., Mecham, R.P., Boak, L.K.S.B.B., Eichwald, E., Keating, M.T., 1998. Elastin is an essential determinant of arterial morphogenesis. Nature 393 (6682), 276–280.

Lopez-Candales, A., Holmes, D.R., Liao, S., Scott, M.J., Wickline, S.A., Thompson, R.W., 1997. Decreased vascular smooth muscle cell density in medial degeneration of human abdominal aortic aneurysms. Am. J. Pathol. 150, 993–1007.

Maier, A., Essler, M., Gee, M.W., Eckstein, H.H., Wall, W.A., Reeps, C. Correlation of biomechanics to tissue reaction in aortic aneurysm assessed by finite elements and 18F-fluordeoxyglucose-PET/CT. Int. J. Numer. Methods Biomed. Eng., in press, doi:10.1002/cnm.1477.

Malek, A.M., Izumo, S., 1995. Control of endothelial cell gene expression by flow. J. Biomech. 28, 1515–1528.

Martufi, G., Di Martino, E.S., Amon, C.H., Muluk, S.C., Finol, E.A., 2009. Three-dimensional geometrical characterization of abdominal aortic aneurysms: image-based wall thickness distribution. J. Biomech. Eng. 131, 061015.

Menashi, S., Campa, J.S., Greenhalgh, R.M., Powell, J.T., 1987. Collagen in abdominal aortic aneurysm: Typing, content, and degradation. J. Vasc. Surg. 6, 578–582.

Mohan, S., Mohan, N., Valente, A.J., Sprague, E.A., 1999. Regulation of low shear flow-induced HAEC VCAM-1 expression and monocyte adhesion. Am. J. Physiol. Cell Physiol. 276, c1100-7.

Mulvany, M.J., 1992. Vascular growth in hypertension. J. Cardiovasc. Pharmacol. 20, S17-S11.

Raghavan, M., Vorp, D., 2000. Toward a biomechanical tool to evaluate rupture potential of abdominal aortic aneurysm: identification of a finite strain constitutive model and evaluation of its applicability. J. Biomech. 33, 475–482.

Raghavan, M.L., Vorp, D.A., Federle, M.P., Makaroun, M.S., Webster, M.W., 2000. Wall stress distribution on three-dimensionally reconstructed models of human abdominal aortic aneurysm. J. Vasc. Surg. 31, 760–769.

Please cite this article in press as: Zeinali-Davarani, S., Baek, S., Medical image-based simulation of abdominal aortic aneurysm growth. Mech. Re. Commun. (2012), doi:10.1016/j.mechrescom.2012.01.008

Rissland, P., Alemu, Y., Einav, S., Ricotta, J., Bluestein, D., 2009. Abdominal aortic aneurysm risk of rupture: patient-specific FSI simulations using anisotropic model. J. Biomech. Eng. 131, 031001.
Rizvi, M.A.D., Katwa, L., Spadone, D.P., Myers, P.R., 1996. The effects of endothelin-1 on collagen type i and type iii synthesis in cultured porcine coronary artery vascular smooth muscle cells. J. Mol. Cell Cardiol. 28, 243–252.
Rizzo, R.J., McCarthy, W.J., Dixit, S.N., Lilly, M.P., Shively, V.P., Flinn, W.R., Yao, J.S.T., 1989. Collagen types and matrix protein content in human abdominal aortic aneurysms. J. Vasc. Surg. 10 (4), 365–373.
Sacks, M.S., Vorp, D.A., Raghavan, M.L., Federle, M.P., Webster, M.W., 1999. In vivo three-dimensional surface geometry of abdominal aortic aneurysms. Ann. Biomed. Eng. 27, 469–479.
Scotti, C.M., Shkolnik, A.D., Muluk, S.C., Finol, E.A., 2005. Fluid–structure interaction in abdominal aortic aneurysms: effects of asymmetry and wall thickness. Biomed. Eng. Online 4 (64), 1L 22.
Sheidaei, A., Hunley, S.C., Zeinali-Davarani, S., Raguin, L.G., Baek, S., 2011. Simulation of abdominal aortic aneurysm growth with updating hemodynamic loads using a realistic geometry. Med. Eng. Phys. 33, 80–88.
Shum, J., Di Martino, E.S., Goldhammer, A., Goldman, D.H., Acker, L.C., Patel, G., Ng, J.H., Martufi, G., Finol, E.A., 2010. Semiautomatic vessel wall detection and quantification of wall thickness in computed tomography images of human abdominal aortic aneurysms. Med. Phys. 37, 638–648.
Shum, J., Martufi, G., Di Martino, E.S., Washington, C.B., Grisafi, J., Muluk, S.C., Finol, E.A., 2011. Quantitative assessment of abdominal aortic aneurysm geometry. Ann. Biomed. Eng. 39 (1), 277–286.
Speelman, L., Bohra, A., Boosman, E.M.H., Schurink, G.H.W., van de Vosse, F.N., Makaroun, M.S., Vorp, D.A., 2007. Effects of wall calcifications in patient-specific wall stress analyses of abdominal aortic aneurysms. J. Biomech. Eng. 129 (1), 105–109.
Sumner, D.S., Hokanson, D.E., Strandness, D.E., 1970. Stress-strain characteristics and collagen-elastin content of abdominal aortic aneurysms. Surg. Gynecol. Obstet. 130 (3), 459–466.
Sumpio, B.E., Banes, A.J., Link, W.G., Johnson, G.J., 1988. Enhanced collagen production by smooth muscle cells during repetitive mechanical stretching. Arch. Surg. 123, 1233–1236.
Thompson, R.W., Liao, S.X., Curci, J.A., 1997. Vascular smooth muscle cell apoptosis in abdominal aortic aneurysms. Coron. Artery Dis. 8, 623–631.
Thubrikar, M.J., Robicsek, F., Labrosse, M., Chervenkoff, V., Fowler, B.L., 2003. Effect of thrombus on abdominal aortic aneurysm wall dilation and stress. J. Cardiovasc. Surg. 44, 67–77.
Vande Geest, J.P., Sacks, M.S., Vorp, D.A., 2006. The effects of aneurysm on the biaxial mechanical behavior of human abdominal aorta. J. Biomech. 39, 1324–1334.
Vorp, D.A., Lee, P.C., Wang, D.H.J., Makaroun, M.S., Nemoto, E.M., Ogawa, S., Webster, M.W., 2001. Association of intraluminal thrombus in abdominal aortic aneurysm with local hypoxia and wall weakening. J. Vasc. Surg. 34 (2), 291–299.
Vorp, D.A., Raghavan, M.L., Webster, M.W., 1998. Stress distribution in abdominal aortic aneurysm: influence of diameter and asymmetry. J. Vasc. Surg. 27, 632–639.
Walpola, P.L., Gotlieb, A.I., Langille, B.L., 1993. Monocyte adhesion and changes in endothelial-cell number, morphology, and F-actin distribution elicited by low shear-stress in vivo. Am. J. Pathol. 142, 1392–1400.
Wang, D.H.J., Makaroun, M.S., Webster, M.W., Vorp, D.A., 2002. Effect of intraluminal thrombus on wall stress in patient-specific models of abdominal aortic aneurysm. J. Vasc. Surg. 36, 598–604.
Watton, P., Hill, N., Heil, M., 2004. A mathematical model for the growth of the abdominal aortic aneurysm. Biomech. Model Mechanobiol. 3, 98–113.
Watton, P.N., Hill, N.A., 2009. Evolving mechanical properties of a model of abdominal aortic aneurysm. Biomech. Model Mechanobiol. 8 (1), 25–42.
Zeinali-Davarani, S., Raguin, L.G., Baek, S., 2011a. An inverse optimization approach toward testing different hypotheses of vascular homeostasis using image-based models. Int. J. Struct. Changes Solids 3 (2), 33–45.
Zeinali-Davarani, S., Raguin, L.G., Vorp, D.A., Baek, S., 2011b. Identification of in vivo material and geometric parameters of a human aorta: toward patient-specific modeling of abdominal aortic aneurysm. Biomech. Model Mechanobiol. 10, 689–699.
Zeinali-Davarani, S., Sheidaei, A., Baek, S., 2011c. A finite element model of stress-mediated vascular adaptation: application to abdominal aortic aneurysms. Comput. Methods Biomech. Biomed. Eng. 14 (9), 803–817.
Zulliger, M.A., Rachev, A., Stergiopulos, N., 2004. A constitutive formulation of arterial mechanics including vascular smooth muscle tone. Am. J. Physiol. Heart Circ. Physiol. 287 (3), H1335–H1343.

Please cite this article in press as: Zeinali-Davarani, S., Baek, S., Medical image-based simulation of abdominal aortic aneurysm growth. Mech. Re. Commun. (2012), doi:10.1016/j.mechrescom.2012.01.008